Progress In Electromagnetics Research, PIER 56, 129–150, 2006

ON THE PROBLEM WITH INTERMODAL DISPERSION WHEN USING MULTICONDUCTOR TRANSMISSION LINES AS DISTRIBUTED SENSORS

M. Norgren

Div. of Electromagnetic Theory, Alfvén Laboratory, Kungliga Tekniska Högskolan
Teknikringen 31, SE-100 44, Stockholm, Sweden

Abstract—The inverse problem of using an unshielded multiconductor transmission line (MTL) as an distributed sensor is considered. The MTL is analyzed by means of the quasi-TEM mode theory and a propagator formalism. In the inverse problem, the focus is on the problem with intermodal dispersion, due to the possibility of more than one propagating mode. Reconstruction results, from both measured and simulated reflection data, are presented for a three conductor MTL that has been used for diagnosing soil and snow. Both the case when one mode propagates, and the case when two modes propagate are considered. For the latter case it is demonstrated that intermodal dispersion deteriorates the resolution in the reconstruction, due to corruption of the high frequency part of the spectrum.

1. INTRODUCTION

The inverse problem of parameter reconstruction on nonuniform transmission lines is of importance in various sensor applications. For example, bulk media can be diagnosed using the reflection/transmission data from submerged unshielded transmission lines, which have been designed so that their propagation characteristics are strongly sensitive to the properties of the surrounding media. In [1, 2] a multi-conductor transmission line (MTL) in the form of a flat three conductor bandcable has been used to characterize the properties of soil or snow. From measured reflection data the shunt-capacitance can be reconstructed as a function of the position along the cable, whereby one can infer information about e.g., water content and density of the medium.

There are several factors which determine the feasibility and quality of the reconstruction. Such factors are e.g., uncertainties

in the parameters which are considered as known. For example, when diagnosing dielectric media, the series inductance and the series resistance of the cable must be known with good accuracy. Another limiting factor is the smallest possible resolution length, which is roughly half of the wavelength corresponding to the maximum frequency that can be used. Normally, transmission lines operate in the quasi-TEM mode regime, which ranges from DC up to frequencies where the wavelengths starts to be comparable with the cross-sectional dimensions of the line. For unshielded MTL:s the usable frequency range may be reduced further, due to radiation losses, especially if the MTL is long in terms of wavelengths or badly matched at the load end.

Reconstructing the parameters of a nonuniform transmission line is a formidable task, see e.g., [3, 4], and to the best knowledge of the author the reconstruction algorithms that have been developed so far are all restricted to single mode (scalar) transmission line models. However, an MTL with $N + 1$ conductors supports N quasi-TEM modes, which in general propagate with different velocities. Hence, a pulse built up of several modes will suffer from intermodal dispersion as it propagates along the MTL. In the construction of devices utilizing MTL:s, intermodal dispersion can be suppressed by designing the feed, load, and junctions so that only one mode exists in each section of the MTL. In such situations, a single mode reconstruction algorithm can be used. For example, in [1, 2] the reconstruction algorithms are based on that only the even mode propagates along the three conductor cable.

However, when submerged into an unknown medium there is no guarantee that only one mode will be excited on the MTL. When surrounded by e.g., a homogeneous medium, a three conductor symmetric band-cable supports one even mode and one odd mode, but if the surrounding medium is heterogeneous and asymmetric over the width of the cable (see the right portion in Figure 1) hybrid modes (which are neither even nor odd) will instead propagate. Thus, in the sensor application the modes are in general not known a priori, and therefore one cannot eliminate undesired modes by matching. Due to the intermodal dispersion, one can expect that undesired modes will degrade the quality of a reconstruction based on a single mode algorithm. In the present paper, we examine critically how intermodal dispersion influences the quality of the reconstruction. As a suitable object, we consider the band-cable used in [1, 2], on which we have performed measurement to verify the theoretical results.

The paper is organized as follows: In Section 2, we recapture the basic properties of the quasi-TEM modes and derive the scattering parameters and propagators that are used for the analysis of the band-cable. In Section 3, we describe the measurement setup and

calculate the parameters of the band-cable. In Section 4, we present reconstruction results for symmetric MTL:s, with only a single mode propagating, and for asymmetric MTL:s, suffering from intermodal dispersion because of two propagating modes. Section 5 contains the conclusions.

Figure 1. (left) Band-cable and surrounding medium realizing a symmetric MTL, supporting an even and an odd mode. (right) Band-cable and surrounding medium realizing an asymmetric MTL, supporting two hybrid modes.

2. THE QUASI-TEM MODES

For details about the quasi-TEM mode theory, we refer to [5–7]. Since we in this study only consider MTL:s with small losses, we initially restrict the analysis to the lossless case. The losses are estimated in Section 3.1.2.

Consider an MTL with $N+1$ conductors. One conductor is chosen as the reference, assigned zero-valued electric and magnetic potentials. For the cable considered in the experiment, the center conductor is the reference; see figure 1. All properties of the quasi-TEM modes can be derived from two $N \times N$-matrices $\boldsymbol{L}$ and $\boldsymbol{C}$: the inductance and capacitance (per unit length) matrices. The n:th mode is described by its wave number β_n and two vectors, $\boldsymbol{u}_n$ and $\boldsymbol{i}_n$, whose components are the voltages and currents on the conductors. The wave number and the voltage and current vectors follow from the eigenvalue equations

$$\left[(\boldsymbol{LC})^{1/2} - \frac{\beta_n}{\omega}\mathcal{I}\right]\boldsymbol{u}_n = 0 \tag{1}$$

$$\left[(\boldsymbol{CL})^{1/2} - \frac{\beta_n}{\omega}\mathcal{I}\right]\boldsymbol{i}_n = 0 \tag{2}$$

where $\mathcal{I}$ is the identity matrix. The matrix square roots $(\boldsymbol{LC})^{1/2}$ and

$(\boldsymbol{CL})^{1/2}$ are transposes of each other, and thus share the same set of eigenvalues, $\{\beta_n\}_{n=1}^N$, but the sets of eigenvectors $\{\boldsymbol{u}_n\}_{n=1}^N$ and $\{\boldsymbol{i}_n\}_{n=1}^N$ are different in general. For all modes, the voltage and current vectors are related through the relations

$$\boldsymbol{u}_n = \boldsymbol{Z}\boldsymbol{i}_n, \qquad \boldsymbol{i}_n = \boldsymbol{Y}\boldsymbol{u}_n \tag{3}$$

where the impedance matrix $\boldsymbol{Z}$ and its inverse $\boldsymbol{Y}$ are

$$\boldsymbol{Z} = (\boldsymbol{LC})^{1/2}\,\boldsymbol{C}^{-1}, \qquad \boldsymbol{Y} = (\boldsymbol{CL})^{1/2}\,\boldsymbol{L}^{-1} \tag{4}$$

The quasi-TEM modes can be shown to be orthogonal in the power sense, and the modal voltage and current vectors are assumed to have been orthonormalized, so that

$$\boldsymbol{u}_m^\top \boldsymbol{i}_n = \boldsymbol{u}_m^\top \boldsymbol{Y}\boldsymbol{u}_n = \boldsymbol{i}_m^\top \boldsymbol{Z}\boldsymbol{i}_n = \delta_{mn} \tag{5}$$

Let $\hat{\boldsymbol{U}}$ and $\hat{\boldsymbol{I}}$ be matrices whose columns are the normalized voltage and current eigenvectors, respectively. Thus, we have

$$\hat{\boldsymbol{U}} = \boldsymbol{Z}\hat{\boldsymbol{I}}, \qquad \hat{\boldsymbol{I}} = \boldsymbol{Y}\hat{\boldsymbol{U}} \tag{6}$$

$$\hat{\boldsymbol{U}}^\top \hat{\boldsymbol{I}} = \hat{\boldsymbol{I}}^\top \hat{\boldsymbol{U}} = \mathcal{I} \tag{7}$$

The total voltages and currents, propagating in both directions along the line, are

$$\boldsymbol{U}(x) = \sum_{n=1}^{N} \boldsymbol{u}_n \left(a_n^+ \mathrm{e}^{-\mathrm{j}\beta_n x} + a_n^- \mathrm{e}^{+\mathrm{j}\beta_n x} \right) \tag{8}$$

$$\boldsymbol{I}(x) = \sum_{n=1}^{N} \boldsymbol{i}_n \left(a_n^+ \mathrm{e}^{-\mathrm{j}\beta_n x} - a_n^- \mathrm{e}^{+\mathrm{j}\beta_n x} \right) \tag{9}$$

where the coefficients $a_n^\pm$ are determined from the excitation and loading conditions. Introducing the x-dependent coefficient vectors

$$\boldsymbol{a}^\pm(x) = \begin{bmatrix} a_1^\pm \mathrm{e}^{\mp\mathrm{j}\beta_1 x} \\ \vdots \\ a_N^\pm \mathrm{e}^{\mp\mathrm{j}\beta_N x} \end{bmatrix} \tag{10}$$

the voltage and current vectors can be written compactly as

$$\boldsymbol{U}(x) = \hat{\boldsymbol{U}} \left(\boldsymbol{a}^+(x) + \boldsymbol{a}^-(x) \right) \tag{11}$$

$$\boldsymbol{I}(x) = \hat{\boldsymbol{I}} \left(\boldsymbol{a}^+(x) - \boldsymbol{a}^-(x) \right) \tag{12}$$

Using (7), the coefficient vectors are obtained from the voltage and the current as

$$\boldsymbol{a}^{+}(x) = \frac{1}{2}\left(\hat{\boldsymbol{I}}^{\top}\boldsymbol{U}(x) + \hat{\boldsymbol{U}}^{\top}\boldsymbol{I}(x)\right) \tag{13}$$

$$\boldsymbol{a}^{-}(x) = \frac{1}{2}\left(\hat{\boldsymbol{I}}^{\top}\boldsymbol{U}(x) - \hat{\boldsymbol{U}}^{\top}\boldsymbol{I}(x)\right) \tag{14}$$

2.1. Scattering Parameters

Consider two N-conductor transmission lines, which are connected with each other in the cross-sectional plane $x = x_0$. Let region 1 be in $x < x_0$ and region 2 in $x > x_0$.

The coupling between the modes can be described by scattering matrices, defined from the relations

$$\begin{bmatrix} \boldsymbol{a}_1^{-}(x_0) \\ \boldsymbol{a}_2^{+}(x_0) \end{bmatrix} = \begin{bmatrix} \boldsymbol{S}_{11} & \boldsymbol{S}_{12} \\ \boldsymbol{S}_{21} & \boldsymbol{S}_{22} \end{bmatrix} \begin{bmatrix} \boldsymbol{a}_1^{+}(x_0) \\ \boldsymbol{a}_2^{-}(x_0) \end{bmatrix} \tag{15}$$

Using (11), (12) and the conditions $\boldsymbol{U}_1\left(x_0^{-}\right) = \boldsymbol{U}_2\left(x_0^{+}\right), \boldsymbol{I}_1\left(x_0^{-}\right) = \boldsymbol{I}_2\left(x_0^{+}\right)$ for the voltage and the current, the scattering matrices become

$$\boldsymbol{S}_{11} = \left(\hat{\boldsymbol{U}}_2^{\top}\hat{\boldsymbol{I}}_1 + \hat{\boldsymbol{I}}_2^{\top}\hat{\boldsymbol{U}}_1\right)^{-1}\left(\hat{\boldsymbol{U}}_2^{\top}\hat{\boldsymbol{I}}_1 - \hat{\boldsymbol{I}}_2^{\top}\hat{\boldsymbol{U}}_1\right) \tag{16}$$

$$\boldsymbol{S}_{12} = 2\left(\hat{\boldsymbol{U}}_2^{\top}\hat{\boldsymbol{I}}_1 + \hat{\boldsymbol{I}}_2^{\top}\hat{\boldsymbol{U}}_1\right)^{-1} \tag{17}$$

$$\boldsymbol{S}_{21} = 2\left(\hat{\boldsymbol{U}}_1^{\top}\hat{\boldsymbol{I}}_2 + \hat{\boldsymbol{I}}_1^{\top}\hat{\boldsymbol{U}}_2\right)^{-1} \tag{18}$$

$$\boldsymbol{S}_{22} = \left(\hat{\boldsymbol{U}}_1^{\top}\hat{\boldsymbol{I}}_2 + \hat{\boldsymbol{I}}_1^{\top}\hat{\boldsymbol{U}}_2\right)^{-1}\left(\hat{\boldsymbol{U}}_1^{\top}\hat{\boldsymbol{I}}_2 - \hat{\boldsymbol{I}}_1^{\top}\hat{\boldsymbol{U}}_2\right) \tag{19}$$

It can be shown that the total scattering matrix is symmetric, i.e.

$$\boldsymbol{S}_{11} = \boldsymbol{S}_{11}^{\top}, \qquad \boldsymbol{S}_{22} = \boldsymbol{S}_{22}^{\top}, \qquad \boldsymbol{S}_{21} = \boldsymbol{S}_{12}^{\top} \tag{20}$$

In the above derivation we have not regarded the mismatch between the modal field-patterns at the different sides of the plane $x = x_0$. To properly satisfy the field boundary conditions higher order evanescent modes must be added, which can approximately be modelled as lumped elements between the conductors at x_0. In this study, the conductors have no geometrical discontinuities along the MTL, wherefore we assume that higher modes may be neglected in the frequency range where the quasi-TEM theory is adequate.

2.2. Propagator for the Voltage and the Current

If the voltage and current are known at the location x along a uniform line, the voltage and current at the location $x+\Delta x$ can be determined easily by means of a propagator:

$$\begin{bmatrix} \boldsymbol{U}(x+\Delta x) \\ \boldsymbol{I}(x+\Delta x) \end{bmatrix} = \boldsymbol{P}(\Delta x) \begin{bmatrix} \boldsymbol{U}(x) \\ \boldsymbol{I}(x) \end{bmatrix} \tag{21}$$

To determine the propagator matrix $\boldsymbol{P}(\Delta x)$, we first note that the phase-shifts in the mode coefficients are given as

$$\boldsymbol{a}^{\pm}(x+\Delta x) = \mathcal{D}^{\pm}(\Delta x)\, \boldsymbol{a}^{\pm}(x) \tag{22}$$

where the diagonal matrices $\mathcal{D}^{\pm}(\Delta x)$ are

$$\mathcal{D}^{\pm}(\Delta x) = \operatorname{diag}\left\{ \mathrm{e}^{\mp \mathrm{j}\beta_1 \Delta x}, \cdots, \mathrm{e}^{\mp \mathrm{j}\beta_N \Delta x} \right\} \tag{23}$$

Using (13) and (14), (22), (11) and (12), it follows that

$$\boldsymbol{P}(\Delta x) = \begin{bmatrix} \hat{\boldsymbol{U}}\, \mathcal{C}(\Delta x)\, \hat{\boldsymbol{I}}^{\top} & -\mathrm{j}\hat{\boldsymbol{U}}\, \mathcal{S}(\Delta x)\, \hat{\boldsymbol{U}}^{\top} \\ -\mathrm{j}\hat{\boldsymbol{I}}\, \mathcal{S}(\Delta x)\, \hat{\boldsymbol{I}}^{\top} & \hat{\boldsymbol{I}}\, \mathcal{C}(\Delta x)\, \hat{\boldsymbol{U}}^{\top} \end{bmatrix} \tag{24}$$

where

$$\begin{aligned} \mathcal{C}(\Delta x) &= \operatorname{diag}\left\{ \cos(\beta_1 \Delta x), \cdots, \cos(\beta_N \Delta x) \right\} \\ \mathcal{S}(\Delta x) &= \operatorname{diag}\left\{ \sin(\beta_1 \Delta x), \cdots, \sin(\beta_N \Delta x) \right\} \end{aligned}$$

The inverse of the propagator matrix (the back-propagator) becomes

$$\left[\boldsymbol{P}\left(\Delta x\right)\right]^{-1} = \boldsymbol{P}\left(-\Delta x\right) = \begin{bmatrix} \hat{\boldsymbol{U}}\, \mathcal{C}(\Delta x)\, \hat{\boldsymbol{I}}^{\top} & \mathrm{j}\hat{\boldsymbol{U}}\, \mathcal{S}(\Delta x)\, \hat{\boldsymbol{U}}^{\top} \\ \mathrm{j}\hat{\boldsymbol{I}}\, \mathcal{S}(\Delta x)\, \hat{\boldsymbol{I}}^{\top} & \hat{\boldsymbol{I}}\, \mathcal{C}(\Delta x)\, \hat{\boldsymbol{U}}^{\top} \end{bmatrix} \tag{25}$$

For a line consisting of several different sections, the continuity of the voltage and the current makes it straightforward to cascade the individual propagators into a total propagator. For a line with M sections located between $x_0, x_1, x_2, \ldots, x_{M-1}, x_M$, the total propagator from x_0 to x_M becomes

$$\boldsymbol{P}_{\mathrm{tot}} = \boldsymbol{P}_M(x_M - x_{M-1}) \cdots \boldsymbol{P}_2(x_2 - x_1)\, \boldsymbol{P}_1(x_1 - x_0) \tag{26}$$

3. THE MEASUREMENT SETUP AND THE BAND-CABLE

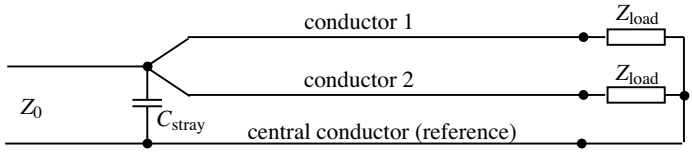

Figure 2. Schematic picture of the measurement setup.

The measurement setup, given schematically in Figure 2, was designed so that only the even mode was launched when the MTL was symmetric. The length of the band-cable was 2.00 m. The cable was terminated with two lumped resistors $R_{\text{load}} = 390\ \Omega$, between the central conductor to each of the outer conductors; see Figure 3(a). Near the load end we can expect an increased pile up of charges on the conductors, which yields an extra amount of capacitance near the load. These capacitances has been estimated to be $C_{\text{load}} \approx 0.23\,\text{pF}$ for each of the conductors. The load impedances thus become approximately

$$Z_{\text{load}} = \frac{R_{\text{load}}}{1 + \text{j}\omega R_{\text{load}} C_{\text{load}}} \tag{27}$$

Hence, the load impedance seen by the even mode becomes $Z_{\text{load}}/2$, which was the value that was used in the reconstructions algorithm.

The measurements were performed with an HP8510C/HP8517A network analyzer system. The feeding coaxial cable from the network analyzer has a characteristic impedance $Z_0 = Y_0^{-1} = 50\ \Omega$. At the feeding end the outer conductors of the band-cable are attached to the screen of the coaxial connector via two wires which are approximately 2 cm in length; see Figure 3(b). At the feeding point, these wires yield an increased amount of shunt capacitance, which is modelled as a lumped capacitor with the estimated value $C_{\text{stray}} \approx 1.45\,\text{pF}$.

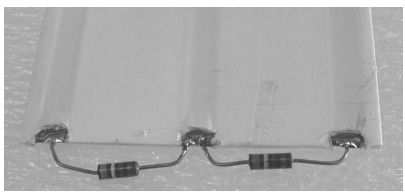

(a) The load resistors.

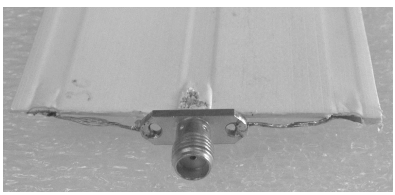

(b) The coaxial connector.

Figure 3. The termination and feeding of the band-cable.

To find the reflection coefficient, we proceed as follows: the relation between the voltages and currents at the load end becomes $\boldsymbol{U}_{\text{load}} = \boldsymbol{Z}_{\text{load}}\boldsymbol{I}_{\text{load}}$, where the impedance matrix

$$\boldsymbol{Z}_{\text{load}} = \begin{bmatrix} Z_{\text{load}} & 0 \\ 0 & Z_{\text{load}} \end{bmatrix} \tag{28}$$

Let $\boldsymbol{B} = \boldsymbol{P}_{\text{tot}}^{-1}$ be the back-propagator from the load-end to the feeding-end Splitting $\boldsymbol{B}$ into 2×2 sub-matrices, we obtain

$$\begin{bmatrix} \boldsymbol{U}_{\text{in}} \\ \boldsymbol{I}_{\text{in}} \end{bmatrix} = \begin{bmatrix} \boldsymbol{B}_{UU} & \boldsymbol{B}_{UI} \\ \boldsymbol{B}_{IU} & \boldsymbol{B}_{II} \end{bmatrix} \begin{bmatrix} \boldsymbol{Z}_{\text{load}}\boldsymbol{I}_{\text{load}} \\ \boldsymbol{I}_{\text{load}} \end{bmatrix} \tag{29}$$

Eliminating $\boldsymbol{I}_{\text{load}}$, the current vector at the feeding end becomes

$$\boldsymbol{I}_{\text{in}} = \left[\boldsymbol{B}_{IU}\boldsymbol{Z}_{\text{load}} + \boldsymbol{B}_{II}\right]\left[\boldsymbol{B}_{UU}\boldsymbol{Z}_{\text{load}} + \boldsymbol{B}_{UI}\right]^{-1}\boldsymbol{U}_{\text{in}} \tag{30}$$

where in our case

$$\boldsymbol{U}_{\text{in}} = U_{\text{in}}\begin{bmatrix} 1 \\ 1 \end{bmatrix}, \qquad \boldsymbol{I}_{\text{in}} = \begin{bmatrix} I_{\text{in},1} \\ I_{\text{in},2} \end{bmatrix}$$

The scalar input admittance seen from the supplying line then becomes

$$Y_{\text{in}} = \frac{I_{\text{in},1} + I_{\text{in},2}}{U_{\text{in}}} + \mathrm{j}\omega C_{\text{stray}} \tag{31}$$

wherefrom the reflection coefficient becomes

$$\Gamma = \frac{Y_0 - Y_{\text{in}}}{Y_0 + Y_{\text{in}}} \tag{32}$$

3.1. Calculation of the Parameters of the Flat Band-Cable

A three-conductor symmetric cable supports two quasi-TEM modes, the odd mode and the even mode, which each can be described by scalar parameters L, C, R, G. For the present cable, the insulation is made of polyethylene with a relative permittivity about 2.25. Since the losses in the polyethylene are very small, the shunt conductance is neglected completely, i.e. $G = 0$.

The series resistance R is due to the finite conductivity of the copper conductors. Since the conductivity $\sigma = 5.7 \cdot 10^7$ S/m is large, we expect small losses, i.e. $R \ll \omega L$. In such a case, one can first compute the parameters L and C from a lossless model of the cable; R is then calculated by a perturbation technique.

3.1.1. The Series Inductance and the Shunt Capacitance

For a flat-band cable surrounded by air, calculations using a commercial numerical software gives the following inductance and capacitance matrices:

$$\boldsymbol{L} = \begin{bmatrix} 1.17 & 0.44 \\ 0.44 & 1.17 \end{bmatrix} \mu\text{H/m}, \qquad \boldsymbol{C} = \begin{bmatrix} 12.6 & -4.5 \\ -4.5 & 12.6 \end{bmatrix} \text{pF/m} \quad (33)$$

wherefrom the velocities and normalized voltage- and current-vectors for the two modes become

$$v_1 = 2.83 \cdot 10^8 \text{ m/s}, \quad \boldsymbol{u}_1 = \begin{bmatrix} -10.2 \\ 10.2 \end{bmatrix} \Omega^{1/2}, \quad \boldsymbol{i}_1 = \begin{bmatrix} -0.0492 \\ 0.0492 \end{bmatrix} \Omega^{-1/2}$$

$$v_2 = 2.75 \cdot 10^8 \text{ m/s}, \quad \boldsymbol{u}_2 = \begin{bmatrix} 14.9 \\ 14.9 \end{bmatrix} \Omega^{1/2}, \quad \boldsymbol{i}_2 = \begin{bmatrix} 0.0335 \\ 0.0335 \end{bmatrix} \Omega^{-1/2}$$

Mode 1 is an odd mode and mode 2 is an even mode. From the proportionality between $\boldsymbol{u}_1$ and $\boldsymbol{i}_1$, and $\boldsymbol{u}_2$ and $\boldsymbol{i}_2$, respectively, the modes can be described by scalar voltages, currents and characteristic impedances. The voltages and currents are defined as

$$\begin{aligned} U_{\text{odd}} &= [\boldsymbol{u}_1]_2 - [\boldsymbol{u}_1]_1, & I_{\text{odd}} &= [\boldsymbol{i}_1]_2 = -[\boldsymbol{i}_1]_1 \\ U_{\text{even}} &= [\boldsymbol{u}_2]_1 = [\boldsymbol{u}_2]_2, & I_{\text{even}} &= [\boldsymbol{i}_1]_1 + [\boldsymbol{i}_1]_2 \end{aligned}$$

whereby the characteristic impedances become

$$Z_{\text{odd}} = 414\ \Omega, \qquad Z_{\text{even}} = 223\ \Omega$$

From the mode velocities and the relations $L = Z/v, C = 1/(Zv)$, the series inductances and shunt capacitances for the modes become

$$\begin{aligned} L_{\text{odd}} &= 1.46\ \mu\text{H/m}, & C_{\text{odd}} &= 8.5\ \text{pF/m} \\ L_{\text{even}} &= 810\ \text{nH/m}, & C_{\text{even}} &= 16.3\ \text{pF/m} \end{aligned}$$

3.1.2. The Series Resistance

With $G = 0$, the characteristic impedance and the propagation factor become [8]

$$Z = \sqrt{\frac{\text{j}\omega L + R}{\text{j}\omega C}} \quad (34)$$

$$\gamma = \alpha + \text{j}\beta = \sqrt{(\text{j}\omega L + R)\,\text{j}\omega C} \quad (35)$$

With $R \ll \omega L$, R usually can be neglected in the expression (34) for the characteristic impedance. Hence, we set $Z = \sqrt{L/C}$, which is the same as for a lossless line. However, in (35) the attenuation factor α is due to R which can therefore not be neglected. Using $R \ll \omega L$, one obtains approximately

$$\alpha \approx \frac{R}{2Z}, \qquad \beta \approx \omega\sqrt{LC}. \tag{36}$$

The voltage, current and power propagating in the $+x$-direction can be written

$$U(x) = ZI_0\mathrm{e}^{-\gamma x}, \qquad I(x) = I_0\mathrm{e}^{-\gamma x}, \tag{37}$$

$$P(x) = \mathrm{Re}\left\{U(x)\,I^*(x)\right\} = Z\,|I_0|^2\,\mathrm{e}^{-2\alpha x}. \tag{38}$$

The power per unit length delivered to the conductors thus becomes

$$P_\mathrm{l} = -\frac{\mathrm{d}P\,(x)}{\mathrm{d}x} = 2\alpha Z\,|I_0|^2\,\mathrm{e}^{-2\alpha x} = R\,|I_0|^2\,\mathrm{e}^{-2\alpha x} = R\,|I|^2 \tag{39}$$

The copper conductors have the width $w = 5\,\mathrm{mm}$ and the thickness $t = 0.15\,\mathrm{mm}$. For very low frequencies, when the penetration depth $\delta = \sqrt{2/\left(\omega\sigma\mu_0\right)}$ satisfies $\delta \gg t$, the current becomes nearly uniformly distributed over the conductor cross-sections, which yields

$$P_\mathrm{l} = \frac{1}{\sigma w t}\sum_{i=0}^{N}|I_i|^2 \tag{40}$$

(subscript 0 refers to the reference conductor). For the even mode, we have $|I_\mathrm{l}| = |I_\mathrm{r}| = |I|/2, |I_\mathrm{c}| = |I|$, whilst for the odd mode we have $|I_\mathrm{l}| = |I_\mathrm{r}| = |I|\,, I_\mathrm{c} = 0$, which yields

$$R^\mathrm{DC}_\mathrm{even} = \frac{3}{2\sigma w t} \approx 35\ \mathrm{m\Omega/m}, \qquad R^\mathrm{DC}_\mathrm{odd} = \frac{2}{\sigma w t} \approx 47\ \mathrm{m\Omega/m} \tag{41}$$

As the frequency increases the current becomes more and more concentrated towards the surfaces of the conductors. For intermediate frequencies, when $\delta \approx t$, the analysis becomes difficult. However, for higher frequencies, when $\delta \ll t$, the power loss can be computed by means of a surface resistance model. With the surface resistance $R_\mathrm{s} = 1/\left(\sigma\delta\right)$ [8], the power loss per unit length becomes

$$P_\mathrm{l} = R_\mathrm{s}\sum_{i=0}^{N}\oint_{\mathcal{C}_i}|\boldsymbol{K}|^2\,\mathrm{d}l, \tag{42}$$

where $\boldsymbol{K}$ is the surface current density, and the integral is taken around the circumferences of the conductors. The surface current density is determined from the same magnetostatic problem that was solved numerically when determining the inductance matrix. Let $\hat{\boldsymbol{n}}$ denote the inward unit normal at the surfaces of the conductor. From the magnetic field $\boldsymbol{B}$ and its vector potential $\boldsymbol{A} = A\hat{\boldsymbol{x}}$, one obtains

$$\begin{aligned} \boldsymbol{K} &= -\frac{1}{\mu_0}\hat{\boldsymbol{n}} \times \boldsymbol{B} = -\frac{1}{\mu_0}\hat{\boldsymbol{n}} \times (\nabla \times \boldsymbol{A}) \\ &= -\frac{1}{\mu_0}\hat{\boldsymbol{n}} \times (\nabla A \times \hat{\boldsymbol{x}}) = \frac{1}{\mu_0}(\hat{\boldsymbol{n}} \cdot \nabla A)\,\hat{\boldsymbol{x}} = \frac{\hat{\boldsymbol{x}}}{\mu_0} \cdot \frac{\partial A}{\partial n} \end{aligned} \tag{43}$$

The expression (42) for the power loss per unit length in the conductors thus becomes

$$P_{\mathrm{l}} = \frac{R_{\mathrm{s}}}{\mu_0^2} \sum_{i=0}^{N} \oint_{\mathcal{C}_i} \left(\frac{\partial A}{\partial n}\right)^2 \mathrm{d}l, \tag{44}$$

whilst the total current flowing in each of the conductors becomes

$$I_i = \oint_{\mathcal{C}_i} \boldsymbol{K} \cdot \hat{\boldsymbol{x}} \mathrm{d}l = \frac{1}{\mu_0} \oint_{\mathcal{C}_i} \frac{\partial A}{\partial n} \mathrm{d}l, \quad i = 0, \ldots N. \tag{45}$$

Identifying the total current in the mode and using (44), the series resistance as defined by (39) can be written in the form

$$R = \xi R_{\mathrm{s}}, \tag{46}$$

where the factor ξ has the following values for the even and odd mode, respectively:

$$\xi_{\mathrm{even}} \approx 214 \text{ m}^{-1}, \qquad \xi_{\mathrm{odd}} \approx 288 \text{ m}^{-1} \tag{47}$$

The corresponding series resistances as functions of the frequency are given in Figure 4. In Figure 5, the attenuation $\mathrm{e}^{-\alpha l}$ due to R is given as functions of the frequency for a 2 m cable and a 20 m cable. For the short cable the attenuation is small and thus hardly detectable in an experiment. For the longer cable, on the other hand, one sees that the series resistance has a non-negligible contribution to the attenuation.

To check the results in (47), we compare with an approximate analytical result given by Collin [8]: for an isolated single conductor of width w and thickness t one has

$$\xi_{\mathrm{Collin}} = \frac{\pi + \ln(4\pi w/t)}{\pi^2 w}, \quad t/w < 0.05 \tag{48}$$

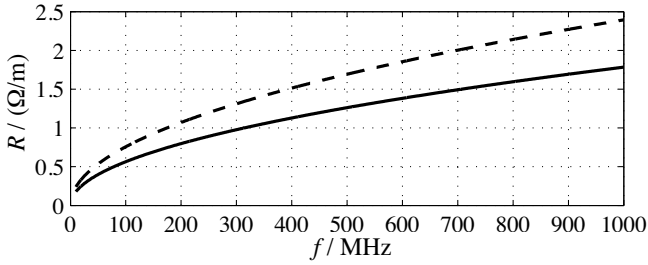

Figure 4. The series resistance of the band-cable. Even mode - solid line; odd mode - dashed line.

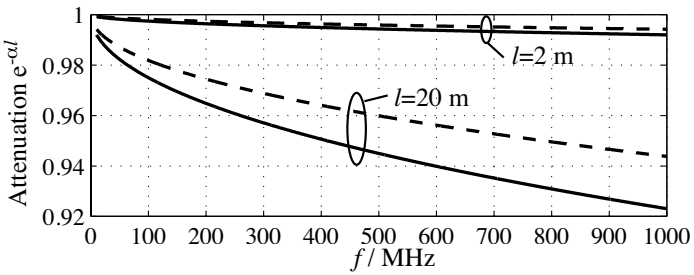

Figure 5. The attenuation due to the series resistance, for cables with lengths 2 m and 20 m respectively. Even mode - solid lines; odd mode - dashed lines.

In our case $t/w = 0.03$, which yields $\xi_{\text{Collin}} \approx 186\ \text{m}^{-1}$. Neglecting the interaction between the conductors, one then obtains

$$\xi_{\text{even}} \approx \frac{3}{2}\xi_{\text{Collin}} \approx 279\ \text{m}^{-1}, \qquad \xi_{\text{odd}} \approx 2\xi_{\text{Collin}} \approx 372\ \text{m}^{-1}$$

The differences against (47) may partly be explained by convergence problems in the numerical calculations. Since the conductors are thin, the singular behavior of the fields in the vicinity of the edges yields a poor numerical convergence, even though local mesh-refinement has been used. Nevertheless, the numerical and analytical results indicate the order of the magnitude of the series resistance.

3.2. Measured Parameters

In [1], the following measured values were reported for the reactive parameters of the even mode:

$$L_{\text{even}}^{\text{meas}} = 756 \text{ nH/m}, \qquad C_{\text{even}}^{\text{meas}} = 17.6 \text{ pF/m}$$

In our own calibration measurements, we obtained values very close to the above ones. Some of the differences from the numerically obtained values in Section 3.1.1 may be attributed to the afore-mentioned convergence problem in the numerical calculations.

Since the maximum length of the cables we made measurements upon was 2 m, we conclude from Figure 5 that it is difficult to determine the series resistance R from these measurements. Also, this kind of open cable radiates, whereby the radiation losses (which have not been included in the model) may dominate over the losses due to R.

4. RECONSTRUCTIONS FROM MEASURED AND SIMULATED REFLECTION DATA

In the experiments, we constructed transmission lines with different capacitance matrices by sandwiching the flat band-cable between blocks of either Plexiglas or polyethylene. Consulting [9] and [10] respectively, the relative permittivities have the nominal values given in Table 1. These materials have negligible losses, wherefore we keep the value $G = 0$ for the shunt conductance.

Table 1. Nominal values of the relative permittivities for the dielectric media around the cable.

	Plexiglas	Polyethylene
ε_{r}	2.6	2.35

4.1. Symmetric Lines with the Even Mode Only

In the first experiment, a 775 mm section of the cable was sandwiched between two blocks of Plexiglas; see Figure 6. The thickness of the Plexiglas was 24 mm. The order and lengths of the sections were

$$\text{| air } 500\,\text{mm} \text{ | Plexiglas } 775\,\text{mm} \text{ | air } 725\,\text{mm} \text{ |}$$

In the Plexiglas section, the numerically obtained value of the shunt capacitance for the even mode is $C_{\text{even}}^{\text{plexi}} = 33.4$ pF/m.

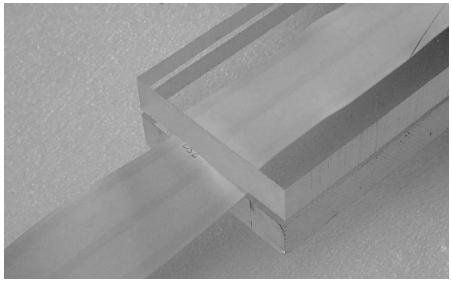

Figure 6. The flat band-cable sandwiched between two blocks of Plexiglas.

For the reconstructions, we used the conjugate gradient based optimization method described in e.g., [11]. When reconstructing from measured data we used the value $L = 756\ \mu$H/m [1] for the series inductance, and when reconstructing from simulated data we used the calculated value $L = 810\,\mu$H/m. Note that in this case the single-mode reconstruction algorithm is applicable, since (in the ideal case) the excitation-, termination- and scattering-conditions guarantee that only the even mode will exist along the line.

In all reconstructions we used measurement data and simulation data from 633 evenly spaced frequencies from 45 MHz to 800 MHz. The upper limit of the frequency range is chosen in order to avoid problems with radiation from the cable and the lower limit is dictated by the networker analyser system. A procedure which in practice has proved to reduce the problem with local minima in the optimization method is to start with low-frequency data only and reconstruct essentially the mean values of the parameters. Then, one gradually incorporate data from higher frequencies to reconstruct the fine structure. For the sake of comparison, all figures with reconstruction results are given in the same scale.

The results in this first case are depicted in Figure 7. From the prior knowledge that the permittivity of the surrounding media is piecewise constant, we see that the reconstructions are successful. The boundaries of the blocks of Plexiglas are located correctly and elsewhere the profiles tend to fluctuate around piecewise constant values. The reconstruction from simulated data practically recovers the calculated values of the even mode capacitances.

In the second experiment, one section of the cable was sandwiched between the same two blocks of Plexiglas which were used in the first experiment. Another section of the cable was sandwiched between two blocks of polyethylene. The order and lengths of the sections were

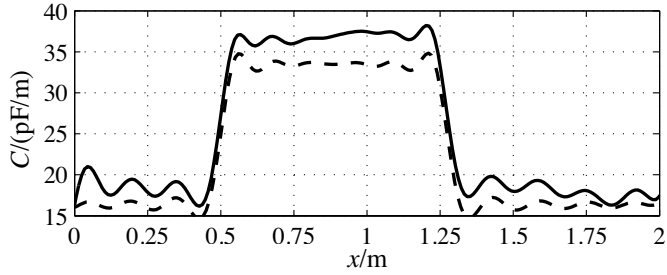

Figure 7. Reconstruction of shunt capacitance along a cable sandwiched between Plexiglas in $0.500\,\mathrm{m} < x < 1.275\,\mathrm{m}$: from measured data (solid line); from simulated data (dashed line).

| air 250 mm | Plexiglas 775 mm | air 275 mm | polyethylene 358 mm | air 342 mm |

In the polyethylene section, the numerically obtained value of the shunt capacitance for the even mode is $C_{\mathrm{even}}^{\mathrm{poly}} = 30.8$ pF/m. The results of the reconstructions are depicted in Figure 8.

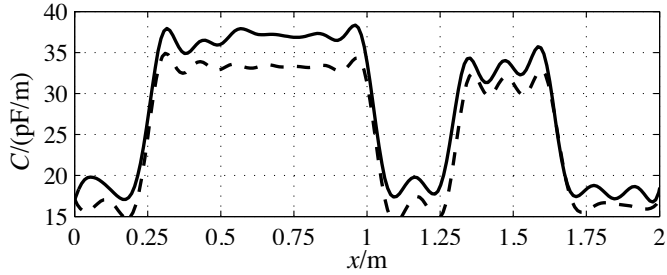

Figure 8. Reconstruction of shunt capacitance along a cable sandwiched between plexiglass in $0.250\,\mathrm{m} < x < 1.025\,\mathrm{m}$ and polyethylene in $1.300\,\mathrm{m} < x < 1.658\,\mathrm{m}$: from measured data (solid line); from simulated data (dashed line).

4.2. Dispersion Due to Multiple Modes

Before doing the reconstructions using data contaminated from intermodal dispersion, we make an approximate estimate about the influence when two modes are present on the cable. The propagation velocities for the modes are $v_n = \omega/\beta_n$. Due to the boundary

conditions at the feeding end, a launched signal splits into several modes, which in general propagate with different velocities. Hence, the dispersion due to multiple modes must be considered. In applications where the length of the cable is shorter than the wavelength, intermodal dispersion is not likely to be a problem, but (as can be seen from the previous reconstructions) the present application requires several wavelengths along the cable, in order to obtain a good resolution. Hence, intermodal dispersion sets an upper(lower) limit on the frequencies(pulse rise-times) which can be used.

Assume two modes which propagate with the velocities v_1 and v_2 respectively. Let Δx denote the desired spatial resolution along the cable, and define the relative difference between the velocities as $\Delta v / \langle v \rangle$, where $\Delta v = |v_1 - v_2|$ and $\langle v \rangle = \sqrt{v_1 v_2}$. The required rise-time (or pulse-width) then approximately becomes

$$\Delta t = \frac{\Delta x}{\langle v \rangle} \tag{49}$$

Let l denote the length of the cable. For pulses belonging to two different modes, with velocities v_1 and v_2 respectively, the difference between the arrival-times after propagation forth and back along the cable becomes

$$\delta t = \left| \frac{2l}{v_1} - \frac{2l}{v_2} \right| = \frac{2l\Delta v}{\langle v \rangle^2} \tag{50}$$

Intermodal dispersion should be negligible if $\delta t \ll \Delta t$, which yields

$$\frac{\Delta v}{\langle v \rangle} \ll \frac{\Delta x}{2l} \tag{51}$$

That is, the relative difference between the velocities certainly must be much less than the relative resolution, $\Delta x / l$, along the cable.

In a frequency domain formulation, the condition for neglecting intermodal dispersion is that the difference in the phase-progressions forth and back along the line satisfies

$$2l \left| \beta_1 - \beta_2 \right| = 2l \cdot 2\pi f \left| \frac{1}{v_1} - \frac{1}{v_2} \right| \ll \pi \tag{52}$$

which yields

$$\frac{\Delta v}{\langle v \rangle} \ll \frac{\langle v \rangle}{4fl} = \frac{\langle \lambda \rangle / 2}{2l} \tag{53}$$

where $\langle \lambda \rangle$ is the average wavelengths between the modes. Note that (53) conforms with the time-domain result (51), since $\langle \lambda \rangle / 2$ is the

required resolution corresponding to Δx. Expressed as a limitation of the frequency, (53) becomes

$$f \ll \frac{\langle v \rangle^2}{4l\Delta v} \tag{54}$$

4.3. Asymmetric Lines with Two Modes Present

When used for diagnosing snow, airgaps around the cable may develop due to melting, re-freezing of the snow and vibrations of the cable. With a vertically oriented cross-section, airgaps may develop asymmetrically (Figure 9), giving rise to hybrid modes along the cable.

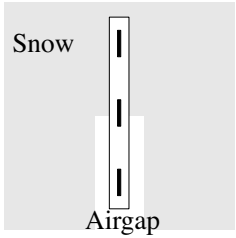

Figure 9. Surrounding medium with an airgap over half of the cable cross-section.

4.3.1. Region with Airgap over Half of the Cable-Width

We emulated an airgap over half of the cable cross-section by inserting corrugated carton between the cable and the Plexiglas. In the numerical calculation the airgap was void. The overall width of the airgap, over both sides of the cable, was 9 mm.
The MTL studied had the following sections:

| air 500 mm | Plexiglas with partial airgap 775 mm | air 725 mm |

The calculated capacitance matrix for the section with a partial airgap becomes

$$\boldsymbol{C} = \begin{bmatrix} 24.4 & -7.7 \\ -7.7 & 18.5 \end{bmatrix} \text{ pF/m}$$

The inductance matrix, which is unaffected by dielectric media, is given in Section 3.1.1. The velocities and normalized voltage- and current-

vectors for the two modes become

$$v_1 = 2.32 \cdot 10^8 \text{ m/s}, \quad \boldsymbol{u}_1 = \begin{bmatrix} 2.1 \\ 16.0 \end{bmatrix} \Omega^{1/2}, \quad \boldsymbol{i}_1 = \begin{bmatrix} -0.0168 \\ 0.0648 \end{bmatrix} \Omega^{-1/2}$$

$$v_2 = 2.00 \cdot 10^8 \text{ m/s}, \quad \boldsymbol{u}_2 = \begin{bmatrix} 15.2 \\ 3.9 \end{bmatrix} \Omega^{1/2}, \quad \boldsymbol{i}_2 = \begin{bmatrix} 0.0681 \\ -0.0089 \end{bmatrix} \Omega^{-1/2}$$

Clearly, these modes are neither even nor odd. Mode 1, has the fields more concentrated to the airgap region and thereby a greater velocity than mode 2, for which the fields are more concentrated into the region where the Plexiglas adheres to the cable. Furthermore, the voltage- and current-vectors in the respective modes are not proportional, but related via the impedance matrix

$$\boldsymbol{Z} = \begin{bmatrix} 234 & 93 \\ 93 & 270 \end{bmatrix} \Omega$$

With subscript 1 denoting the air-region adjacent to the feeding end and subscript 2 denoting the Plexiglas-region, the scattering matrices at $x = 500\,\text{mm}$ become

$$\boldsymbol{S}_{11} = \begin{bmatrix} -0.130 & 0.036 \\ 0.036 & -0.126 \end{bmatrix}, \qquad \boldsymbol{S}_{22} = \begin{bmatrix} 0.092 & -0.007 \\ -0.007 & 0.164 \end{bmatrix},$$

$$\boldsymbol{S}_{21} = \boldsymbol{S}_{12}^{\top} = \begin{bmatrix} 0.748 & 0.657 \\ -0.649 & 0.743 \end{bmatrix}$$

In $\boldsymbol{S}_{21}, \boldsymbol{S}_{12}$, one sees that an incident mode splits up in two transmitted modes with quite equal magnitudes.

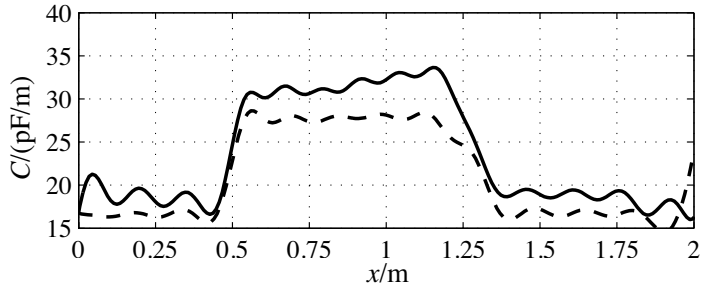

Figure 10. Reconstruction of shunt capacitance from measured data (solid line) and simulated data (dashed line).

The reconstructions, using the single-mode reconstruction algorithm, are depicted in Figure 10. Comparing with the reconstructions from data that is not contaminated from intermodal dispersion (Figures 7 and 8) we see in Figure 10 that the some of the steepness has been lost where the discontinuities are located (especially at the rear end of the Plexiglas section), which is a clear indication that high-frequency information has been lost due to the intermodal dispersion.

4.3.2. Region with Plexiglas over Half of the Cable-Width

In the second asymmetric case we consider a cable with two adjacent sections sandwiched between Plexiglas, but in the first section the cable is only covered over half of its with; see Figure 11. The MTL we studied had the following sections:

| air 500 mm | Plexiglas over half the width 351 mm | Plexiglas 424 mm | air 725 mm |

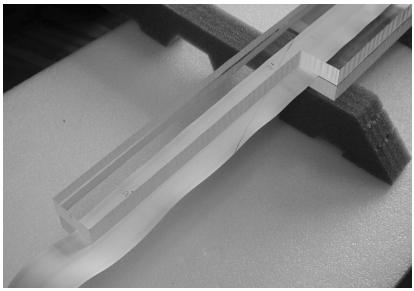

Figure 11. Transition region where the flat band-cable is partly sandwiched between two blocks of Plexiglas.

The calculated capacitance matrix for the asymmetric section becomes

$$\boldsymbol{C} = \begin{bmatrix} 14.0 & -5.9 \\ -5.9 & 22.7 \end{bmatrix} \text{ pF/m}$$

The velocities and normalized voltage- and current-vectors for the two modes become

$$v_1 = 2.66 \cdot 10^8 \text{ m/s}, \quad \boldsymbol{u}_1 = \begin{bmatrix} 16.8 \\ 1.2 \end{bmatrix} \Omega^{1/2}, \quad \boldsymbol{i}_1 = \begin{bmatrix} 0.0609 \\ -0.0191 \end{bmatrix} \Omega^{-1/2}$$

$$v_2 = 2.05 \cdot 10^8 \text{ m/s}, \quad \boldsymbol{u}_2 = \begin{bmatrix} 4.8 \\ 15.5 \end{bmatrix} \Omega^{1/2}, \quad \boldsymbol{i}_2 = \begin{bmatrix} -0.0049 \\ 0.0662 \end{bmatrix} \Omega^{-1/2}$$

and the impedance matrix becomes

$$\boldsymbol{Z} = \begin{bmatrix} 306 & 96 \\ 96 & 241 \end{bmatrix} \Omega$$

The scattering matrices at the interface between the first air-section and the section partly covered with Plexiglas are

$$\boldsymbol{S}_{11} = \begin{bmatrix} -0.080 & -0.063 \\ -0.063 & -0.098 \end{bmatrix}, \qquad \boldsymbol{S}_{22} = \begin{bmatrix} 0.025 & 0.007 \\ 0.007 & 0.152 \end{bmatrix},$$
$$\boldsymbol{S}_{21} = \boldsymbol{S}_{12}^{\top} = \begin{bmatrix} 0.788 & -0.615 \\ 0.607 & 0.800 \end{bmatrix}$$

The reconstructions, using the single-mode algorithm, are depicted in Figure 12. Comparing with Figures 7 and 8 we see also in this second asymmetric case that some of the expected steepness at the discontinuities has been lost due to the intermodal dispersion.

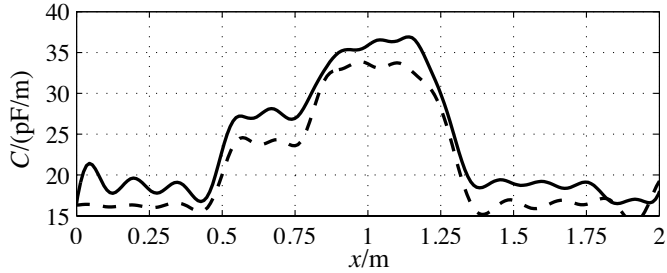

Figure 12. Reconstruction of shunt capacitance from measured data (solid line) and simulated data (dashed line).

5. DISCUSSION AND CONCLUSIONS

A three-conductor flat band-cable, used for diagnosing purposes in soil and snow, has been analyzed by means of the quasi-TEM mode theory. Comparing the reconstructions from measured data with the ones from simulated data, we conclude that the quasi-TEM mode theory is appropriate for the analysis of this kind of transmission line. The results for the transmission line parameters show that the series resistance must be taken into account when using long cables in sensor applications.

The reconstructions from both measured and simulated reflection data show that a high resolution can be obtained if there is only one

mode that propagates along the MTL, which usually is the case when the medium surrounding the cable has a symmetric distribution. For the asymmetric MTL:s, the presence of two modes and the intermodal dispersion clearly degrades the reconstruction results; the smoothing of the discontinuous profiles is more pronounced due to the loss of high frequency information. Hence, the existence of several modes cannot be overlooked when considering an MTL as a distributed sensor. In a practical case, one thus needs prior information about the possible existence of inhomogeneities in the cross-section of the MTL.

ACKNOWLEDGMENT

The author is grateful to Dr. Peter Fuks for valuable discussions and assistance with the measurements. This work was funded by a grant from The Fifth Framework Programme of the European Commission, and their support is gratefully acknowledged.

REFERENCES

1. Hübner, C., "Entwicklung hochfrequenter Meßverfahren zur Boden- und Schneefeuchtebestimmung," Ph.D. thesis, Institut für Meteorologie und Klimatforschung, Forschungszentrum Karlsruhe, Karlsruhe, Germany, 1999.
2. Schlaeger, S., "Inversion von TDR-Messungen zur Rekonstruktion rumlich verteilter bodenphysikalischer parameter," Ph.D. thesis, Institutes für Bodenmechanik und Felsmechanik der Universit"at Fridericiana in Karlsruhe, Karlsruhe, Germany, 2002.
3. Lundstedt, J. and S. Ström, "Simultaneous reconstruction of two parameters from the transient response of a nonuniform LCRG transmission line," *J. Electro. Waves Applic.*, Vol. 10, 19–50, Jan. 1996.
4. Frangos, P. V. and D. L. Jaggard, "Inverse scattering: Solution of coupled Gel'fand-Levitan-Marchenko integral equations using succesive kernel approximations," *IEEE Trans. Antennas Propagat.*, Vol. AP-43, 547–552, June 1995.
5. Lindell, I. V., "On the quasi-TEM modes in inhomogeneous multiconductor transmission lines," *IEEE Trans. Microwave Theory Tech.*, Vol. MTT-29, 812–817, Aug. 1981.
6. Marx, K. D., "Propagation modes, equivalent circuits, and characteristic terminations for multiconductor transmission lines with inhomogeneous dielectrics," *IEEE Trans. Microwave Theory Tech.*, Vol. MTT-21, 450–457, July 1973.

7. Paul, C. R., "Useful matrix chain parameter identities for the analysis of multiconductor transmission lines," *IEEE Trans. Microwave Theory Tech.*, Vol. MTT-23, 756–760, Sept. 1975.
8. Collin, R. E., *Foundations for Microwave Engineering*, second ed., 1992.
9. Afsar, M. N., Y. Wang, and A. Moonshiram, "Measurement of transmittance and permittivity of dielectric material using dispersive fourier transform spectroscopy," *Microwave and Optical Technology Letters*, Vol. 38, 27–30, July 2003.
10. Dorf, R. C. (ed.), *The Electrical Engineering Handbook*, CRC Press, 1993.
11. Norgren, M. and He S., "An optimization approach to the frequency-domain inverse problem for a nonuniform LCRG transmission line," *IEEE Trans. Microwave Theory Tech.*, Vol. 44, 1503–1507, Aug. 1996.